

Spatio-temporal X-wave

Eran Small, Ori Katz, Yochay Eshel, Yaron Silberberg and Dan Oron

Department of physics of Complex System, The Weizmann Institute of Science, Rehovot 76100, Israel

Abstract: We introduce an illumination configuration which is a spatiotemporal analog of a non-diffracting X-wave. By interfering multiple ultrashort converging plane waves, we generate a tight central spot at which a transform limited ultrashort pulse is formed. Outside this tight focus a spatiotemporal speckle field with longer duration and reduced peak power is created. We investigate this spatiotemporal X-wave configuration analytically, numerically, and experimentally demonstrate the effect using two photon excitation fluorescence.

© 2009 Optical Society of America

OCIS codes: (030.6140) Speckle; (070.0070) Fourier optics and signal processing; (320.0320) Ultrastart optics.

References and links

1. J. Durnin, "Exact solutions for nondiffracting beams. I. The scalar theory," *J. Opt. Soc. Am. A* **4**, 651-654 (1987).
2. J. Lu and J. F. Greenleaf, "Nondiffracting X Waves-Exact Solutions to Free-Space Scalar Wave Equation and Their Finite Aperture Realizations," *IEEE Trans. Ultrasonics Ferroelectrics and Frequency Control* **39**, 19-31 (1992).
3. J. Fagerholm, A. T. Friberg, J. Huttunen, D. P. Morgan, and M. M. Salomaa, "Angular-spectrum representation of nondiffracting X waves," *Phys. Rev. E* **54**, 4347-4352 (1996).
4. G. A. Siviloglou, J. Broky, A. Dogariu, and D. N. Christodoulides, "Observation of Accelerating Airy Beams," *Phys. Rev. Lett.* **99**, 213901 (2007).
5. J. Durnin, J. J. Micelli Jr., and J. H. Eberly, "Diffraction free beams," *Phys. Rev. Lett.* **58**, 1499-1501 (1987).
6. T. Wulle and S. Herminghaus, "Nonlinear optics of Bessel beams," *Phys. Rev. Lett.* **70**, 1401-1404 (1993).
7. O. Manela, M. Segev, and D. N. Christodoulides, "Nondiffracting beams in periodic media," *Opt. Lett.* **30**, 2611-2613 (2005).
8. Y. Lahini, Y. Silberberg, S. Droulias, K. Hizanidis, R. Morandotti, and D. N. Christodoulides, "Discrete X-Wave Formation in Nonlinear Waveguide Arrays," *Phys. Rev. Lett.* **98**, 023901 (2007).
9. C. J. R. Sheppard, "Generalized Bessel pulse beams," *J. Opt. Soc. Am. A* **19**, 2218-2222 (2002).
10. O. E. Martinez, "3000 times grating compressor with positive group-velocity dispersion - application to fiber compensation in 1.3-1.6 m region," *IEEE J. Quantum Electronics* **23**, 59 (1987).
11. A. M. Shaarawi, I. M. Besieris, and T. M. Said, "Temporal focusing by use of composite X waves," *J. Opt. Soc. Am. A* **20**, 1658-1665 (2003).
12. D. Oron, E. Tal, and Y. Silberberg, "Scanningless depth resolved microscopy," *Opt. Express* **13**, 1468-1476 (2005).
13. E. Tal and Y. Silberberg, "Transformation from an ultrashort pulse to spatiotemporal speckle by a thin scattering surface," *Opt. Lett.* **31**, 3529-3531 (2006).
14. E. Tal, D. Oron, and Y. Silberberg, "Improved depth resolution in video-rate line-scanning multiphoton microscopy using temporal focusing," *Opt. Lett.* **30**, 1686-1688 (2005).
15. G. Zhu, J. van Howe, M. Durst, W. Zipfel, and C. Xu, "Simultaneous spatial and temporal focusing of femtosecond pulses," *Opt. Express* **13**, 2153-2159 (2005).
16. J. W. Goodman, *Speckle Phenomena in Optics: Theory and application*, (Roberts and Company Publishers, Greenwood village, 2007).
17. J. C Dainty "The statistics of speckle patterns," in progress in optics, Vol XIV, Edited by E. Wolf, North-Holland, Amsterdam, pp 1-44.

1. Introduction

Nondiffracting beams are a general class of infinite energy solutions to the wave equation which, unlike most beams, maintain their spatial profile in the plane perpendicular to their propagation direction. Such "Bessel beams" [1] or "X-waves" [2] are comprised of a coherent summation of plane waves with different propagation directions and appropriate phases such that constructive interference between them is both independent of the propagation coordinate (in the time-averaged intensity sense) and is confined to a relatively small region, corresponding to a relatively localized peak in the intensity [3, 4].

Practical solutions of the wave equation, having finite energy, can only exhibit nearly diffraction-free propagation over finite distances [5]. These still significantly exceed the Rayleigh range of a diffracting beam (such as a Gaussian one) with an equally sized central lobe. Such nondiffracting beams have since been utilized in numerous experimental conditions, such as for nonlinear optics applications [6] and in discrete systems [7, 8].

When dealing with ultrashort pulsed nondiffracting beams, special care has to be taken to consider the interplay between spectral bandwidth and diffraction [2, 9] and the mixing between dispersion and diffraction. In particular, whenever different spectral components are spatially separated, dispersion of geometrical origin can alter the temporal profile of ultrashort pulses. In fact, this effect lies at the basis of prism- or grating- based ultrafast pulse compressors [10]. Such effects are of extreme importance when considering nonlinear optical processes.

Use of geometrical dispersion to induce temporal focusing of a composite nondiffracting beam at a given propagation distance, has been suggested several years ago [11]. Temporal focusing of ultrashort pulses via the use of geometrical dispersion, such that an ultrashort pulse is formed only in a given plane, and propagation away from it introduces group velocity dispersion to it, has recently been used in multiphoton microscopy to confine nonlinear excitation only either to a single plane [12, 13] or to a line [14, 15] perpendicular to the propagation direction.

Here we introduce an illumination configuration which is a spatiotemporal analog of a nondiffracting x-waves. The interference of multiple ultrashort plane waves, through the utilization of geometrical dispersion, generates a tight central spot at which the interference is constructive, generating a high peak power short pulse. Outside this spatial region the interference pattern results in longer excitation with a reduced peak power. Since the average power over the entire region is only slowly varying, this interference pattern can only be detected by a nonlinear measurement, where the signal intensity scales with the average squared power. We demonstrate this effect using two photon excitation fluorescence.

In the following we begin by a theoretical description the system leading to the formation of spatiotemporal x-waves, followed by a full numerical analysis and experimental demonstration.

2. Theoretical analysis

A schematic description of the optical setup used for producing a spatiotemporal x-wave is shown in Fig. 1(a). The system is composed of a diffuser placed at the back focal plane (BFP) of a focusing lens. The diffuser is illuminated by a wide beam of ultrashort pulses Fig. 1(a-i). The ultrashort pulse beam is scattered by each point on the diffuser into a propagating spherical pulse front Fig. 1(a-ii,iii). Upon propagation through the lens each of these spherical fronts is transformed into planar one. The interference of all these planar fronts produces a spatiotemporal x-wave at the lens front focal plane (FFP) Fig. 1(a-iv). The resulting field distribution is of a pulse which is short only around the optical axis at the FFP. In this sense, this setup is quite similar to the first experimental realization of nondiffracting beams, where the diffuser was replaced by a thin circular aperture in an opaque screen [5].

An additional feature of this setup is that due to interference between the different parts of

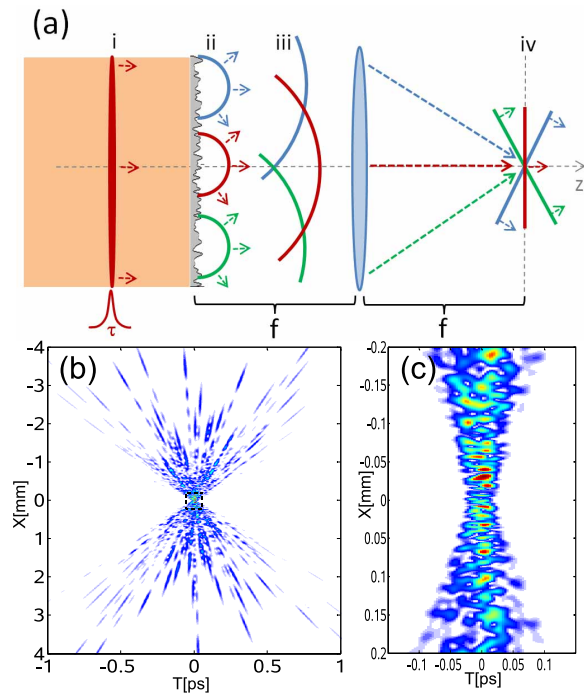


Fig. 1. (a) Scheme of the optical setup used for producing the spatio-temporal x-wave. A wide beam of ultrashort pulses (i) impinges upon a random diffuser placed at the back focal plane of a lens. The ultrashort pulse beam is scattered by the diffuser into multiple propagating spherical wavefronts (ii-iii). The spherical wavefronts are transformed by the lens into converging plane wavefronts, producing a spatio-temporal x-wave on the optical axis at the lens' front focal plane (FFP) (iv). (b) Numerically simulated "snapshot" of the field intensity at the front focal plane of the lens at the x-wave formation time (see text). (c) "Zoom-in" on the center of the x-wave reveals its the spatiotemporal speckle structure.

the scattered beam, the spatial field distribution at any given moment is speckled. The speckle properties are governed by the coherence length of the illuminating beam and the geometry of the optical setup, as will be detailed below. These characteristic are manifested in the "snapshot" image of the X-wave formation given in Fig. 1(b-c), and a movie of the X-wave formation Fig. 2 obtained through numerical simulations (see below).

An alternative approach for understanding the spatiotemporal pattern at the FFP is by analyzing the system as an optical Fourier transform from the BFP ($z = -f$ where the diffuser is located) to the FFP ($z = f$). For a monochromatic input beam, the output is the familiar speckle field, which is the Fourier transform of the diffuser rough surface (phase pattern), scaled by the wavelength (λ). The intensity at each point (x, y) on the FFP corresponds to the spatial Fourier component $(k_x, k_y) = (\frac{2\pi}{f\lambda}x, \frac{2\pi}{f\lambda}y)$. When the input beam is an ultrashort pulse, it possess a wide spectral bandwidth. Each wavelength output is the same Fourier transform pattern, up to re-scaling by λ . Thus, the total output field which is a superposition of the same re-scaled pattern, will seem to be smeared in the radial direction, and will possess sharp speckle features only near the optical axis, where the pulse is also short in time Fig. 3.

In the above intuitive argument we have ignored the fact that each wavelength is mod-

ulated by a different phase mask, therefore a precise calculation will now follow in order to justify that assumption. For a monochromatic beam, the input field after the diffruser, $E(x, y, z = -f)$ Fig. 1(a.i) can be statistically described by its correlation function, $\Gamma(x_1, y_1, x_2, y_2) = \langle E^*(x_1, y_1)E(x_2, y_2) \rangle$ [16], which is given by:

$$\Gamma_\lambda(x_1, y_1; x_2, y_2, z = -f) \simeq I(x_1, y_1)\mu_\lambda(\Delta x, \Delta y) \quad (1)$$

where $\Delta x = (x_1 - x_2)$, $\Delta y = (y_1 - y_2)$, $\mu_\lambda(\Delta x, \Delta y)$ is the correlation function for wavelength λ describing the homogenous diffuser, and $I(x, y)$ is the incident beam's intensity profile (we will assume a gaussian profile with a standard deviation σ). This type of initial correlation is a result of a beam with a non-homogenous profile (dependent on coordinates x, y) which is scattered from a homogenous diffuser, having a correlation function which is dependent only on the relative distances $\Delta x, \Delta y$.

Using the lens' known transformation from BFP to FFP, one can calculate the field's correlation function at the lens' FFP [16]:

$$\Gamma_\lambda(x_1, y_1; x_2, y_2, z = f) = \frac{1}{\lambda f} \int_{-\infty}^{\infty} \int_{-\infty}^{\infty} I(\alpha_2, \beta_2) e^{\frac{-2\pi i}{\lambda f}(\Delta x \alpha_2 + \Delta y \beta_2)} d\alpha_2 d\beta_2 \times \frac{1}{\lambda f} \int_{-\infty}^{\infty} \int_{-\infty}^{\infty} \mu_\lambda(\Delta \alpha, \Delta \beta) e^{\frac{2\pi i}{\lambda f}(x_1 \Delta \alpha + y_1 \Delta \beta)} d\Delta \alpha d\Delta \beta \quad (2)$$

The output field correlation function can be factored into a product of two functions, one is the Fourier transform of the input beam with respect to $(\Delta x, \Delta y)$ and the second is the Fourier transform of the diffuser correlation function with respect to (x_1, y_1) . For an illuminating beam size (σ) much larger than the correlation length of the diffuser, the first function (the Fourier transform of the beam) will be much sharper than the second one (the Fourier transform of the diffuser), and therefore we can approximate the output correlation function as dependent only on the initial illuminating beam profile. As a result the speckle size at the output will be like for a monochromatic beam $\frac{\lambda f}{\sigma}$.

An ultrashort pulse input beam possess a wide wavelength spectrum. Therefore, the output field is the coherent sum of all the speckle patterns generated by the different wavelengths. The pulse temporal shape at each point in space is dictated by the relative amplitude and phases of these speckle patterns. When the phases of these patterns are correlated, as happens on the optical axis, the pulse remains transform-limited (TL). However, as the different wavelengths patterns become uncorrelated, a random spectral phase is obtained, resulting in temporal speckles [13], and hence a longer pulse duration. In order to determine the pulse duration at each point in space, one needs to calculate the correlation between the different wavelengths patterns. On the optical axis all the patterns are completely correlated and the pulse remains TL [17]. In contrast, a point distant by R from the optical axis is associated with the Fourier coefficient $k = \frac{R}{\lambda f}$ and therefore the field at this point will be the sum of different Fourier coefficients for each wavelength. For the pulse to remain short, all the wavelengths in its spectral bandwidth ($\Delta \lambda$) should be associated with Fourier coefficients which are within the correlation length (inside the speckle size in the Fourier plane):

$$\frac{R}{(\lambda - \frac{1}{2}\Delta \lambda)f} - \frac{R}{(\lambda + \frac{1}{2}\Delta \lambda)f} < \frac{1}{\sigma} \quad (3)$$

giving the spatial extent (radii) of the short pulse forming the center of the spatiotemporal X-wave:

$$R < \frac{\lambda}{\Delta \lambda} \left(\frac{\lambda f}{\sigma} \right) \quad (4)$$

It is straightforward to conclude that the X-wave central short pulse contains $\frac{\lambda}{\Delta \lambda}$ individual speckles of size $\frac{\lambda f}{\sigma}$ each.

Similar arguments can be used to estimate the axial (z) extent of the X-wave central short pulse. As the X-wave propagates in the z direction, each wavelength undergoes different fresnel diffraction. The Fresnel-Huygens integral is $E(0, 0, z) = \frac{1}{i\lambda z} \int_{-\infty}^{\infty} E(x, y, 0) e^{\frac{i\pi}{\lambda z}(x^2+y^2)} dx dy$. The correlation at the optical axis is defined as $\Gamma(z) = \langle E_{\lambda_0}(0, 0, z) E_{\lambda_1}^*(0, 0, z) \rangle$ and can be calculated using the fields at the FFP:

$$\Gamma(z) = \frac{1}{\lambda_0 \lambda_1 z^2} \int \int \int \int_{-\infty}^{\infty} \langle E_{\lambda_0}(x_0, y_0, 0) E_{\lambda_1}^*(x_1, y_1, 0) \rangle e^{\frac{i\pi}{\lambda_0 z}(x_0^2+y_0^2) - \frac{i\pi}{\lambda_1 z}(x_1^2+y_1^2)} dx_0 dy_0 dx_1 dy_1 \quad (5)$$

One can define $\lambda_1 = a\lambda_0$ where $a = 1 + \frac{\Delta\lambda}{2\lambda}$ and use re-scaling arguments to get the following relation: $E_{\lambda_1}(x, y, 0) = \frac{1}{a} E_{\lambda_0}(\frac{x}{a}, \frac{y}{a}, 0)$. With the change of variables: $x_2 = \frac{x_1}{\sqrt{a}}, y_2 = \frac{y_1}{\sqrt{a}}$, the correlation can be written as:

$$\Gamma(z) = \frac{1}{a\lambda_0^2 z^2} \int \int \int \int_{-\infty}^{\infty} \langle E_{\lambda_0}(x_0, y_0, 0) E_{\lambda_0}^*(\frac{x_2}{\sqrt{a}}, \frac{y_2}{\sqrt{a}}, 0) \rangle e^{\frac{i\pi}{\lambda_0 z}(x_0^2+y_0^2 - x_2^2 - y_2^2)} dx_0 dy_0 dx_2 dy_2 \quad (6)$$

The correlation for λ_0 at the FFP can be calculated using Eq. (2), and assuming Gaussian beam profile $I(x, y) = I_0 e^{-\frac{x^2+y^2}{2\sigma^2}}$ and Gaussian correlation $\mu(x_2 - x_1, y_2 - y_1) = e^{-\frac{(x_2-x_1)^2 + (y_2-y_1)^2}{2d^2}}$, the correlation function is fully separable:

$$\Gamma(z) = \frac{4\pi^2 \sigma^2 d^2}{a\lambda_0^4 z^2 f^2} \left[\int \int_{-\infty}^{\infty} e^{\frac{i\pi}{\lambda_0 z}(x_0^2-x_2^2)} e^{-\frac{1}{2}(\frac{2\pi d}{\lambda_0 f})^2 x_0^2} e^{-\frac{1}{2}(\frac{2\pi \sigma}{\lambda_0 f})^2 (x_0 - \frac{x_2}{\sqrt{a}})^2} dx_0 dx_2 \right]^2 \quad (7)$$

The analytical solution of the integral under the approximation $d \ll \sigma$ and normalization by the intensity yields:

$$\rho(z) = \frac{\Gamma(z)}{I_{\lambda_0}(0, 0, z)} \simeq \frac{1}{1 + i \frac{\pi \Delta\lambda \sigma^2}{f^2 \lambda^2} z} \quad (8)$$

From Eq. (8) the axial extent of the X-wave central short pulse is obtained:

$$\Delta z_{xwave} \simeq \frac{\lambda^2 f^2}{\pi \Delta\lambda \sigma^2} \quad (9)$$

Where at this length scale the correlation between λ_0 and $\lambda_0 + \Delta\lambda$ decays in a factor of $\sqrt{2}$.

3. Numerical and experimental results

To verify the theoretical predictions, and confirm the formation of a spatiotemporal X-wave, we have studied the pulse evolution throughout the system presented in Fig. 1(a), both numerically and experimentally. We have written a numerical simulation for the pulse evolution using the Fresnel-Huygens propagator under the paraxial approximation. The propagated field was calculated separately for each wavelength in the pulse bandwidth. The fields at the different frequencies were then summed to obtain the temporal profile at each point in space. A movie ([Media 1](#)) summarizing the simulation results, illustrating the pulse evolution throughout the system and the spatiotemporal X-wave formation is given in Fig. 2. The numerical results reveal that after impinging upon the diffuser, the short pulse evolves into a spatiotemporal speckle field whose spherical wavefronts follow the intuitive path depicted in Fig. 1(a). For a system composed of an $f = 5\text{cm}$ lens, 5° diffuser, and a 6mm wide pulse with a central wavelength $\lambda = 810\text{nm}$ and FWHM bandwidth of $\Delta\lambda = 65\text{nm}$, the X-wave center will be composed of a short pulse only $\sim 100\mu\text{m}$ around the optical axis Fig. 1(b). Furthermore, zooming in on the X-wave temporally short center, reveals that it is made up of several spatial speckles Fig. 1(c).

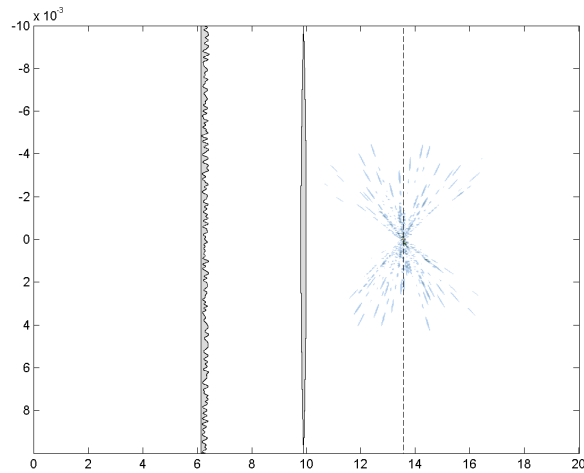


Fig. 2. A movie of the propagation of a pulse through the system. The pulse is longitudinal stretched in order to emphasize its behavior, therefore there seem to be lack of continuously when propagating through the lens. [Media 1](#)

Using Eq. (4) with the above parameters ($\lambda = 810\text{nm}$ and $\Delta\lambda \sim 65\text{nm}$), we expect to get about $\lambda/\Delta\lambda \sim 12$ individual speckles forming the temporal short pulse at the X-wave focus.

To experimentally verify the spatiotemporal X-wave formation, the field distribution both in space and in time has to be measured. This is done by combining linear imaging with nonlinear imaging. The spatial distribution is observed by directly imaging the lens FFP onto a CCD camera. In this case the measured image represents the time averaged intensity at each point in space and therefore contains no information on the pulse temporal shape. To measure the temporal properties we place a thin screen of two-photon absorbing fluorescent dye at different z-positions in the vicinity of the FFP. Since the measured two-photon fluorescent (TPF) intensity is proportional to the integral of the instantaneous field intensity squared, the mean pulse duration at each point in space can be measured from the relative strength of the TPF signal vs. the linear intensity measurement. The experimental setup consisted of a Ti-Sapphire laser oscillator producing ultrashort pulses with a spectral bandwidth of 65nm FWHM. The pulses are passed through a grating compressor to precompensate dispersion. The beam is then magnified to a diameter of 6mm and incident upon a 5° light shaping diffuser (Newport). The scattered beam is focused using an $f = 5\text{cm}$ lens. The TPF screen is a 1mm thick cuvette containing fluorescein dissolved in ethanol. Imaging is performed with a CCD camera (Watec).

Two examples for the experimentally obtained intensity distributions, using the linear imaging setup are given in Fig. 3. Figure 3(a) shows the result obtained using a cw monochromatic beam, producing the well known speckle field, which is the Fourier transform of the diffuser. When illuminating the diffuser with a mode-locked wide bandwidth beam, a radially smeared speckle field, as predicted in the theoretical section Fig. 3(b) is observed. The smeared speckle picture is also a projection of the spatiotemporal speckle field distribution calculated numer-

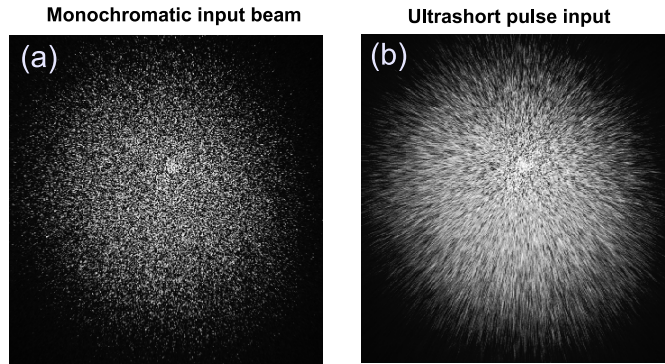


Fig. 3. Experimental linearly imaged speckle pattern at the lens' FFP (Fourier-plane). (a) Ordinary speckle pattern measured using a monochromatic cw incident beam. (b) Radially smeared speckle pattern obtained using an ultrashort pulse incident beam. The radial smearing results from the superimposed re-scaled Fourier images of the wavelengths in the pulse's broad spectrum. The sharp speckles at the center form the X-wave focus which is also temporally short.

ically Fig. 1(b-c). The X-wave center is made of several spatially non-overlapping speckles, which are distinguishable in the linear imaging mode. As we look away from the X-wave center, the spatiotemporal speckles have partial spatial overlap and cannot be resolved using linear (time averaging) imaging, resulting in a smeared pattern. The sharp speckles in the field center are expected to remain short in time, whereas the smeared off-center speckles are expected to be composed of multiple delayed pulses.

The experimental one- and two-photon images (averaged over 10 different diffuser realizations) are shown in Fig. 4(a-b). The radial angle-averaged cross-sections for the two images are plotted in Fig. 4(c). For comparison, the numerically simulated results for the one- and two-photon signals from a spatiotemporal X-wave are plotted in Fig. 4(c). The good agreement between the experimental and numerical result is apparent. The experimental FWHM radii of the one photon signal is ~ 7 times larger than the two photon signal radii, in contrast to the ordinary $\sqrt{2}$ ratio obtained for a Gaussian beam. We can thus conclude that the pulse's temporal width at the center is indeed considerably shorter than away from the optical axis, confirming the spatiotemporal X-wave formation, as theoretically predicted.

A similar strategy was used to study the evolution of the field along the propagation axis. This was done by imaging the field at several different axial (z) positions, shifting the TPF screen from the FFP, for each image. Figure 5 summarizes the experimental results and gives alongside the spatiotemporal X-wave numerical simulation results. One can see that although the average field intensity distribution (given by the linear signal) remains relatively unchanged during propagation, the spatial width of the short temporal pulse (given by the two-photon signal) increases dramatically when moving away from the X-wave focus at the FFP. This result is exactly as expected from the numerical simulation of the X-wave formation process (Fig. 1b-c, MOVIE)

Applying the experimental parameters to Eq. (4) yields an theoretical prediction of $R \simeq 170\mu m$, this result can be verified by experimental results in Fig. 4(b) and Fig. 5(a) (Blue curve), which shows the two photons signal's profile and cross-section. Using Eq. (9) The axial length scale of the X-wave is calculated to be $\Delta z_{xwave} \simeq 1mm$, where the correlation between

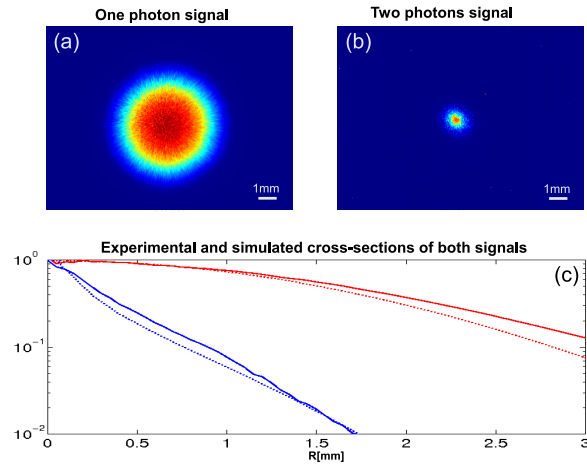


Fig. 4. (a) Linear imaging of the $z = f$ X-wave formation plane averaged over 10 diffuser realizations. Scale bars indicates 1mm. (b) Two-photon image of the same plane, showing an order of magnitude reduced radii confirming the short temporal duration of pulses forming the spatiotemporal X-wave focus. (c) Radial cross-sections of the experimental and simulated signals: red - one photon signals; blue - two photons signals; solid line - experimental signals; dashed line - simulated signals. simulated result

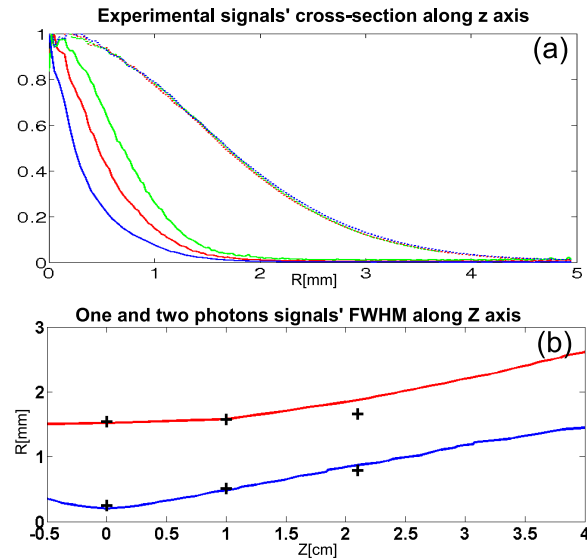


Fig. 5. (a) Experimental one- and two-photon radial cross-sections for planes at several axial (z) positions. Blue - focal plane, red - 10 mm away from the focal plane, green - 21 mm away from the focal plane. Solid line - two photons signal, dotted line - one photon signal. (b) Simulated one- and two-photon radial FWHM as function of axial (z). Red - one photon's FWHM, Blue - Two photons' FWHM. Black crosses mark the experimental FWHM in the measured places

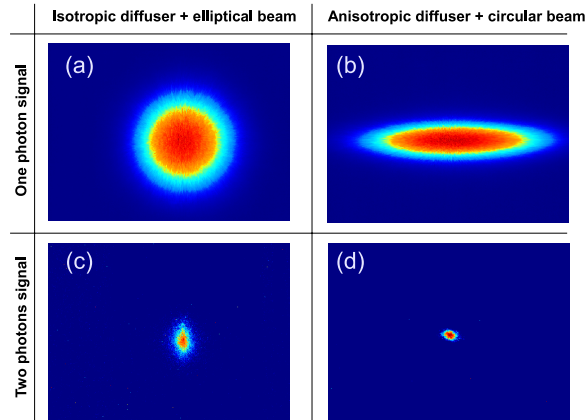


Fig. 6. (a),(c) Experimental one- and two-photon images for an isotropic diffuser and an elliptic (astigmatic) input beam. (b),(d) One- and two-photon images for a anisotropic diffuser and a circular incident beam.

$\lambda_0 = 810nm$ and $\lambda_1 = 840nm$ decays by a factor of $\sqrt{2}$. The correlation between the different wavelengths needed to be $\ll 1$ in order to broaden the pulse, hence we can see the scale of $\sim 5mm$ in a experimental and simulation results in Fig. 5(b).

Re-inspecting Eq. (4), reveals an interesting result: the spatial width of the X-wave short-pulse center is not dependent on the diffuser characteristics. Hence, the two photon signal, which is governed by the pulse temporal width, will not be sensitive to the diffuser roughness and will be determined only by the incident beam parameters. This result is somewhat surprising, as no matter how diffusing is the element placed at the BFP, the TPF image will have the same width. On the other hand the time-averaged speckle field envelope (visualized by regular imaging) is determined solely by the diffuser shape, and is not dependent on the incident beam. Fig. 6 shows the experimental observation of the above conclusions. The one- and two-photon signal were measured in two different setups. The first setup included an isotropic diffuser and an elliptical (astigmatic) input beam Fig. 6(a,c). It can clearly be seen that although the incident beam is elliptical, the one photon signal remains circular but the two photon signal reveals the input beam ellipticity. The second setup included a circular incident beam an anisotropic diffuser (2 degrees in one axis and 10 degrees in the other axis) Fig. 6(b,d). While the linear signal which is governed by the diffuser parameters becomes elliptic, the two photon signal still resembles the isotropic circular input beam.

4. Conclusions

We have shown that an ultrashort pulse scattered by a diffuser positioned at the back focal plane of a lens forms spatiotemporal analog of a non-diffracting x-wave. Each point on the diffuser scatters a diverging impulse that is converted by the lens into a ultrashort plane waves. These plane waves illuminate the entire back focal plane and form a speckle field. We show that these speckles extend over a long time window away from the optical axis, yet they form a tight ultrashort central spot. The radial and longitudinal properties of the pulse were analytically analyzed and the results were verified by numerical simulations. The effect was experimentally tested using one and two photon excitation fluorescence imaging. While one photon excitation is not sensitive to the pulse duration and produces uniform illumination efficiency, two photon

excitation was effective only near the optical axis. These effects that combine diffraction and geometrical dispersion already could be useful in nonlinear microscopy and other applied ultra fast technologies.